Biomaterials 37 (2015) 49–61

Contents lists available at ScienceDirect

Biomaterials

journal homepage: www.elsevier.com/locate/biomaterials

Novel strategy for mechanically tunable and bioactive metal implants

Hyun-Do Jung [a], Tae-Sik Jang [a], Lifeng Wang [c], Hyoun-Ee Kim [a, b], Young-Hag Koh [d, **], Juha Song [a, b, *]

[a] Department of Materials Science and Engineering, Seoul National University, Seoul 151-742, Republic of Korea
[b] Advanced Institutes of Convergence Technology, Seoul National University, Gwanggyo, Yeongtong-gu, Suwon-si, Gyeonggi-do 443-270, Republic of Korea
[c] Department of Mechanical Engineering, 141 Light Engineering, Stony Brook University, Stony Brook, NY 11794, USA
[d] School of Biomedical Engineering, Korea University, Seoul 136-703, Republic of Korea

ARTICLE INFO

Article history:
Received 4 August 2014
Accepted 2 October 2014
Available online 28 October 2014

Keywords:
Sustained drug release
Mechanical tunability
BMP-2
Titanium
Hard tissue engineering

ABSTRACT

Metals have been used as biostructural materials because of outstanding mechanical reliability. However, low bioactivity and high stiffness in biological environments have been major issues of metals, causing stress shielding effects or foreign body reactions after implantation. Therefore, in this study, densified porous titanium has been introduced to achieve comparable mechanical properties to hard tissues and bioactivity that promote a better interface between the implant and bone. Porous titanium scaffolds were successfully fabricated through dynamic freezing casting, and were densified, controlling the degree of densification by applied strain. During densification, structural integrity of porous titanium was well maintained without any mechanical deterioration, exhibiting good pore connectivity and large surface area. Densified porous titanium possesses two important features that have not been achieved by either dense titanium or porous titanium: 1) mechanical tunability of porous scaffolds through densification that allows scaffolds to be applied ranging from highly porous fillers to dense load-bearing implants and 2) improved bioactivity through bioactive coating that is capable of sustainable release through utilizing high surface area and pore connectivity with controllable tortuosity. This simple, but effective post-fabrication process of porous scaffolds has great potential to resolve unmet needs of biometals for biomedical applications.

1. Introduction

Metallic biomaterials have been widely used as load-bearing implants and internal fixation devices such as orthopedic, dental implants, and even vascular/non-vascular stents depending on design because of their excellent mechanical strength and resilience [1–3]. Despite the progress in load-bearing metal implant research, fixation of implants to the host tissue remains a problem. The mismatch between the elastic modulus of the implant material and that of the bone is the main reason that causes the stress to be shielded from reaching the bone in addition to low bioactivity of metallic materials that often leads to poor interface between the implant and biological tissues [4–6]. To overcome these problems, porous structures are being extensively investigated, since a reduction in elastic modulus can be coupled with bone integration through tissue ingrowth into pores to promote healthy recovery [7–9]. Various porous metals such as NiTi, titanium and tantalum have been proved to exhibit strong bone-implant contact and excellent bone ingrowth without signs of loosening from the surgical sites [8,10,11]. Moreover, recent studies have proposed various surface modification methods of metallic surface in order to improve biological activities, e.g., coating the metal surface with bioactive molecules (e.g., growth factors) or drugs (e.g., vancomycin, tetracycline) [12–14]. As compared to bare metals, the bioactive coating layer on a metal surface with or without drugs has shown accelerated healing processes of the implanted region or suppressed undesirable reactions between surrounding tissues and the implant [12,15,16]. These include titanium (Ti) ring implant with recombinant human bone morphogenetic protein (rhBMP-2), e.g., Ti alloy conjugated with synthetic peptide, and Ti screw coated with rhBMP-2 [17–19].

However, introduction of pores to metals has been found to come up with a tradeoff in the mechanical properties besides the reduction of stiffness. Although a porous structure facilitates bone

* Corresponding author. Advanced Institutes of Convergence Technology, Seoul National University, Gwanggyo, Yeongtong-gu, Suwon-si, Gyeonggi-do 443-270, Republic of Korea. Tel.: +82 2 880 8320; fax: +82 2 884 1413.
** Corresponding author. Tel.: +82 2 940 2844; fax: +82 2 909 3502.
E-mail addresses: kohyh@korea.ac.kr (Y.-H. Koh), sat105@snu.ac.kr (J. Song).

http://dx.doi.org/10.1016/j.biomaterials.2014.10.027
0142-9612/

ingrowth, uncontrolled or undesirable pores often result in significant decreases of the mechanical properties due to inherent structural instability associated with irregular, inhomogeneous pore structures and defects [20,21]. Moreover, chemical contamination during the fabrication of porous metals has been found to cause embrittlement of the materials with decreased compressive strength [22–24]. Therefore, development in a fabrication method of porous metals that is able to provide mechanical tunability of a porous scaffold associated with various porosity features (e.g., pore fraction, shape, size, distribution, connectivity and gradient) and material properties (e.g., metallic phase and impurity) has been one of key challenges in order to achieve a balance between biological performance and mechanical stability [10,25].

On the other hand, sustainable release of coating layers on metallic surface has been regarded as an issue of surface modification. Porous metallic implants have been considered as better drug carrier candidates as compared to dense metals because of large surface area. However, porous materials coated with substances experience burst effects in physiological environments, thus methods to control the rate of release is under much research. For example, in attempts to control the initial burst and to sustain the release of substances, nanopores are formed on the surface of implants or polymers with a low degradation rate is used to coat the implants [13,26–28]. However, there are still some room for improvement such as controlling the side-effects caused by the coated polymers, reducing the additional processes needed to form nanopores, and fabricating uniform pore structures [29–31].

In this study, we have proposed densified porous Ti scaffolds as a drug carrier as well as load-bearing implants. The large surface area of the porous scaffolds is capable of loading significantly increased amount of drugs on the metal surface as compared to dense metal body of the same weight [32,33]. In addition, microstructural modification associated with porosity and pore structures of the scaffolds provides mechanical tunability as well as controllable drug release behavior. To demonstrate the potential of porous scaffolds as a drug-loaded metal implant, we have coated porous titanium (Ti) scaffolds with one of well-known bone growth factors, BMP-2. BMP-2 is known to accelerate bone regeneration in the body so it has been widely applied in treatment of bone defects, and also as bioactive coating agents for orthopedic and dental implants [32,34,35]. However, negative side effects including heterotopic bone formation, retrograde ejaculation and osteoclast activation have also been reported with supraphysiologic doses of rhBMP-2 over relatively short periods [31,36–38]. Therefore, many studies have tried to develop a carrier system which is capable of sustained and controlled release of rhBMP-2 over a prolonged period with the bioactivity of the growth factor still maintained [39–41]. Here, we have fabricated porous Ti scaffolds through a dynamic freeze casting process, and coated the scaffolds with rhBMP-2 varying the amount of rhBMP-2 loading with initial porosity. Through densification of the porous scaffolds, modified porosity and pore structures were evaluated in terms of mechanical properties as well as drug release behavior. Moreover, herein, we report for the first time *in vitro* rhBMP-2 release studies for a prolonged period in parallel to *in vivo* study in order to prove biological improvement of rhBMP-2-coated Ti samples.

2. Materials and methods

2.1. Fabrication of densified porous titanium coated with biomolecules

The schematic of sample preparation was illustrated in Fig. 1. In this study, porous Ti scaffold coated with rhBMP-2, a bone growth factor, was studied as a model system for orthopedic applications. Porous Ti scaffolds were fabricated by dynamic freeze casting [42], which enables production of mechanically stable metal scaffolds with 3-dimensionally interconnected porous channels. All samples were sterilized in an autoclave for 15 min at 121 °C. Following the sterilization, the scaffolds were immersed in green fluorescent protein (GFP) or rhBMP-2 solution that had been fabricated using *Escherichia coli* (*E. coli*) [32,43]. Immersed specimens were put into a vacuum desiccator connected to a rotary pump for 10 min, incubated overnight at room temperature (RT), washed with DPBS twice and dried. Subsequently the drug-loaded porous samples were uniaxially compressed in a mold. The initial porosity and degree of densification were major processing parameters used to vary the mechanical properties and to control drug release rates as well as the amount of drug loading.

2.2. Characterization of densified porous titanium

The structures of the dense Ti scaffolds were characterized by scanning electron microscopy (FE-SEM, JSM- 6330, JEOL Techniques, Tokyo, Japan) and μ-computed microtomography (Skyscan 1173 X-ray μ-tomography System, Skyscan, Kontich, Belgium) with the following parameters: 1.0 mm aluminum filter, 180° rotation, 4-frames averaging, 0.2° rotation step, 7.5 μm resolution, 130 kV voltage, and 60 μA current. The pore size was measured and averaged from the SEM images of the samples prepared by filling the porous Ti scaffolds with an epoxy resin (Spurrs epoxy Polysciences Inc., Warrington, PA). The porosity was measured using the volume and mass of the samples in the following equation:

$$p = 100\left(1 - \frac{m_S/V_S}{\rho_{Ti}}\right)$$

where p is the total porosity percentage, ρ_{Ti} is the theoretical density of the titanium and m_S/V_S is the measured density of the sample calculated using the mass (m_S) and volume (V_S). In addition, porosity and pore size were analyzed using computed

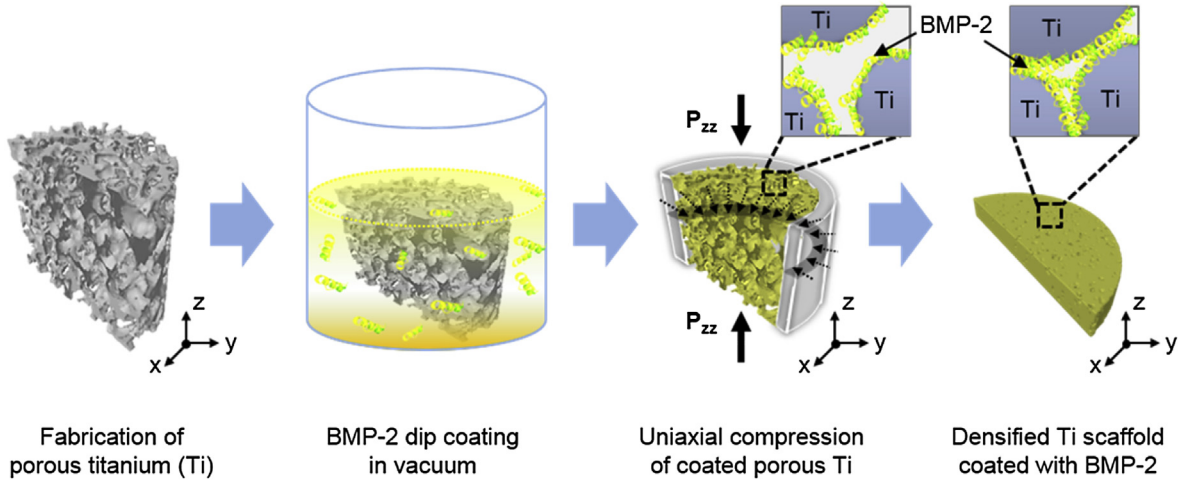

Fig. 1. Schematic illustration of the fabrication process of a densified porous metallic scaffold (Ti) coated with a growth factor (BMP-2). The porous scaffold was compressed under triaxial compression conditions.

microtomography (μ-CT). The acquired images were measured and CTAn (Skyscan, Kontich, Belgium) analysis software analyzed porosity and pore size (details provided in Table 1). The BET surface area of the samples was determined with a Micromeritics by N_2 gas adsorption measurements.

2.3. Mechanical properties of densified porous titanium

The mechanical properties of the porous titanium and densified titanium of various initial porosities were analyzed using Instron 5565 system (Instron, USA) with a cross-head speed of 5 mm/min. The compressive samples were 16.5 mm diameter and 20 mm height. The compressive strengths and stiffness of the samples were obtained from the cyclic compressive loading–unloading curves after load-frame compliance correction.

2.4. Drug release from densified porous titanium

The concentration of rhBMP-2 solution was 100 μg/ml for the *in vitro* release test. The commercial dense titanium and porous titanium specimens were immersed into the prepared rhBMP-2 solution to compare with densified porous titanium. Immersed specimens were put into a vacuum desiccator connected to a rotary pump for 10 min, incubated overnight at 4 °C and washed with DPBS twice. The 3 types of titanium samples with rhBMP-2 (Φ 16 mm *2 mm) were immersed in 5 ml of PBS at 37 °C and pH 7.4 for 140 days. The solutions were suctioned and replenished daily for the first week and weekly for the rest of the experiment. The released rhBMP-2 amounts were measured with UV spectroscopy (ICP-AES, Optima-4300 DV, USA) at 220 nm. A calibration curve was prepared by measuring the optical absorbance of rhBMP-2 in PBS with various concentrations in the range of 0.010–10 μg/ml. The linear relationship between rhBMP-2 concentration and the absorbance was used to quantify rhBMP-2 release. Each absorbance value was directly converted to the amount of rhBMP-2 released using the standard curve. The relative amounts of rhBMP-2 released were normalized to the initially loaded amounts of the titanium scaffolds ($n = 5$). After evaluating the release behavior, the PBS solutions containing the released rhBMP-2 were collected at 2, 4, 6, and 8 weeks into release and were used in cell tests to analyze the functionality of the released rhBMP-2 from the samples.

Similar method as presented for the BMP release was used to visualize the release behavior of the coating layers on three types of Ti samples (commercial dense Ti, porous Ti and densified porous Ti) using GFP. Each Ti sample was immersed into the GFP solution with the concentration of GFP solution of 100 μg/ml for the *in vitro* release test. All immersed specimens were put into a vacuum desiccator connected to a rotary pump for 10 min, incubated overnight at 4 °C and washed with DPBS twice. The GFP coated Ti samples (Φ 16 mm *2 mm) were immersed in 5 ml of PBS at 37 °C and pH 7.4 for 112 days in order to observe the release behavior of the coating layer. The post-release surface fluorescence was observed with confocal laser scanning spectroscopy (CLSM) after immersion for 0, 14, 56 and 112 days.

2.5. Cellular response of released rhBMP-2

The biological activities of the released rhBMP-2 from densified porous Ti were evaluated using the solution containing the released rhBMP-2 at various times. The collected solutions were all diluted to a concentration of 10 ng/ml and were supplemented to the culturing medium to analyze their effects on cell differentiation. A negative control was set as the culturing medium with no rhBMP-2 solution added, and a positive control was set as the culturing medium directly supplemented with fresh rhBMP-2.

The MC3T3-E1 cells were seeded onto the specimens at densities of 2.5×10^3 cells/mL for the proliferation and differentiation tests. The cells were cultured in a humidified incubator with 5% CO_2 at 37 °C. Alpha-minimum essential medium (α-MEM, Welgene Co., Ltd., Korea) that was supplemented with 2% fetal bovine serum (FBS) and 1% penicillin–streptomycin was used as the culturing medium, and 10 mM β-GP and 50 ug/mL ascorbic acid were added for the alkaline phosphatase (ALP) test. The cell differentiation was studied by measuring the ALP activity on day 10. The ALP activity, which indicates the degree of cell differentiation, was measured as an early indicator of the osteoblastic phenotype maintenance using p-nitrophenyl phosphate (pNPP, Sigma–Aldrich, UK). The conversion of pNPP to p-nitrophenol (pNP) in the presence of ALP results in a color change. This colorimetric change can be used to predict the ALP activity since the rate of pNP production is proportional to the ALP activity. A micro-plate reader was used to determine the absorbance at 405 nm. The ALP activity was calculated against a standard curve that was obtained using bovine serum albumin with a concentration ranging from 0.2 to 1.2 mg/mL. The ALP activity test was performed on three samples ($n = 3$) for each condition.

Table 1
Porosity and pore size of the densified Ti scaffolds (I.P.70%) in terms of degree of densification.

Degree of densification	$\varepsilon = 0$	$\varepsilon = 0.35$	$\varepsilon = 0.53$	$\varepsilon = 0.63$	$\varepsilon = 0.66$	$\varepsilon = 0.68$
Porosity [%]	70 ± 1	56 ± 1	33 ± 0	19 ± 0	13 ± 0	7 ± 0
Pore size [μm]	360 ± 30	265 ± 24	150 ± 20	37 ± 10	20 ± 4	12 ± 2

2.6. In vivo implantation

The concentrations of rhBMP-2 solution used for the *in vivo* test were 1 ug/ml. Densified porous titanium with rhBMP-2 was used as the experimental sample and commercial dense titanium and commercial dense titanium coated with rhBMP-2 were used as control samples. The implant was a ring structure measuring 12 mm in diameter, 1.5 mm in thickness, with a 8 mm diameter hole. Six discs per each group were implanted in rabbit calvarias. The animal test was conducted using nine New Zealand white male rabbits (12 weeks old, average weight 3 kg). The animals were weighed at the beginning and at the end of the experiment. All rabbits had a normal diet and were cared under the same conditions. Each animal had two implanted ring implants, one on the upper part and the other on the lower part of the calvaria. With this condition, the three groups of ring implants were distributed among the 9 animals according to a systematic protocol. The surgical sites were shaved and the skin was treated with a surgical prep solution containing 10% povidone-iodine (Betadine). The surgery was performed under conditions of general anesthesia with 0.1 cc of 2% Xylazine HCl (Rompun, Bayer Korea, Korea), 0.2 cc of Tiletamine HCl (Zoletil, Virbac lab, France) and Lidocaine (Yuhan Corporation, Korea). An incision of approximately 4 cm was made at the site of implant placement. A 12 mm diameter trephine bur was used to make two holes through the calvaria on each side of the median calvarial suture and the 12 mm diameter × 1.5 mm ring implants were placed in the holes. The wounds were sutured using Surgisorb (Samyang Ltd, Korea). Gentamicin (0.1 mg/kg SQ) was injected immediately following the operation, then every 24 h for 3 days. Animals were monitored daily for any adverse reaction. 6 weeks following implant placement, the animals were sacrificed by asphyxiation with carbon dioxide. The rabbit calvarias were harvested and the tissues from the implant sites were collected and fixed in 10% neutral-buffered formalin.

2.7. Quantitative microcomputed tomography (μ-CT) evaluation

Following the fixation, the bone volume of new supracalvarial mineralized tissue was analyzed using μ-CT with the following parameters: 0.25 mm brass filter, 180° rotation, 3-frames averaging, 0.2° rotation step, 12 μm resolution, 130 kV voltage, and 60 μA current. The acquired images were processed using a commercial program and the implant morphology and the bone tissues were 3-dimensionally observed using Data viewer (Skyscan, Kontich, Belgium). The gray-scale images were obtained with a fixed threshold to extract the Ti away from the new bone, and the new bone volume was measured using CTAn analysis software.

2.8. Histomorphometrical evaluation

After μ-CT imaging, samples were fixed by immersing in 10% formaldehyde at ambient temperature for several days. Samples were then rinsed in tap water, dehydrated in ethanol and embedded in resin blocks. Applying a systematic random sampling protocol, slices which were randomly cut were prepared from each sample using a diamond saw. Sections were stained with Goldner's trichrome staining. The digital images of the resin block sections were obtained by Axioskop microscopy (Olympus BX51, Olympus Corporation, Japan).

2.9. Statistical analysis

All quantitative data were expressed in terms of mean ± standard deviation (SD) values. One-way ANOVA followed by Bonferroni's post hoc comparison tests were performed in all statistical analyses and $p < 0.05$ was considered significant.

3. Results

3.1. Densification of Ti scaffolds

The porosity of Ti samples was controlled by the degree of densification associated with the applied strain (ε_{zz}) as shown in Fig. 2a. Cylindrical samples with three initial porosities (I.P.) of 50%, 60% and 70% were applied with uniaxial pressure within a mold that constrained radial deformation and only allowed the *z*-axis deformation. The optical image of the sample is shown in terms of degree of densification corresponding to the height of each sample. The heights of the sample decreased as the applied strain (ε_{zz}) increased while the apparent porosity was also significantly reduced. The change of porosity was indicated as a function of strain (ε_{zz}) for three initial porosities where the porous samples were densified up to the final porosity (F.P.) of about 7%. Assuming constant volume for plastic deformation and ignoring the small

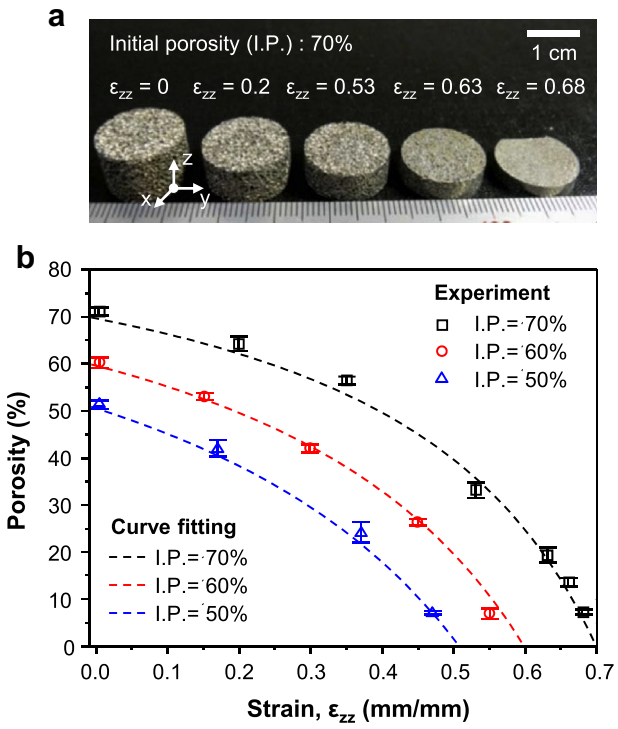

Fig. 2. (a) Optical images of the Ti porous scaffolds (initial porosity (I.P) = 70%) with increased strain (ε_{zz}), and (b) Evolution of porosity with increased strain (ε_{zz}) for Ti porous scaffolds with three initial porosities (50, 60 and 70%).

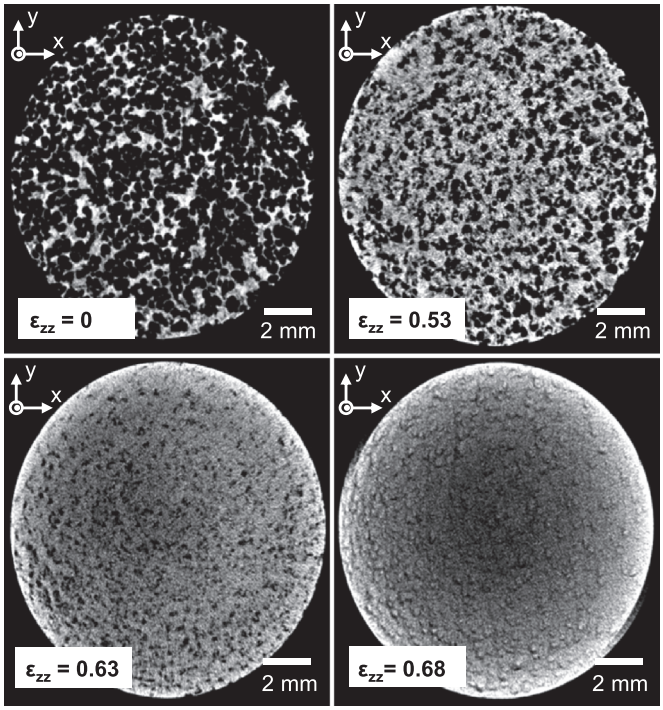

Fig. 3. 2D sectional micro-CT images of the porous Ti scaffolds (I.P. = 70%) at ε_{zz} = 0, 0.53, 0.63 and 0.68.

elastic volume changes, final porosity (F.P.) from densification can be estimated in terms of initial porosity (I.P.) and applied strain (ε_{zz}):

$$\text{F.P.} = 1 - (1 - \text{I.P.})/(1 - \varepsilon_{zz})$$

The experimental F.P. of each sample shows good agreement with predicted values from the above equation as shown in Fig. 2b.

Morphology of internal pores in porous samples was observed depending on the degree of densification, or applied strain (ε_{zz}) using μ-CT images (Fig. 3). The initial pore shape was almost spherical, showing good interconnectivity in the sectioned x-y planes. As densification proceeded, the spherical pores became flattened with narrow gaps. At $\varepsilon_{zz} = 0.68$ (F.P. = 7%), the sectioned plane was likely to be fully densified in which the pores were nearly in contact with each other.

In order to confirm the change of pore interconnectivity caused by densification, total surface areas of three specimens were assessed: commercial titanium and porous titanium scaffold (I.P. = 70%) before and after densification (F.P. = 7%), as shown in Fig. 4a. At the same weight, porous titanium scaffolds possess significantly higher surface area than the dense titanium sample by a factor of approximately 30. Moreover, the microstructure of densified porous scaffold confirmed the gap between metal struts ranges from few tens of micrometers to submicrometers with the average size of ~10 μm, maintaining the interconnectivity of pore channels (Fig. 4b and c). The porosity and pore size of the porous Ti sample (I.P. = 70%) depending on the degree of densification is summarized in Table 1.

3.2. Mechanical tunability of densified Ti scaffolds

The representative stress-strain curves of two porous Ti scaffolds with I.P. = 50% and 70% are shown in Fig. 5a under multiple cycling loading processes with increasing loads. Each cycling loading process gradually densified each porous sample which exhibited increased stiffness and yield strength. During the whole loading process, porous scaffolds were found to be densified without any inconsistent stress-strain behavior because of their comparable ductility to dense Ti, leading to enhanced mechanical properties.

Dependences of the ratios of stiffness on porosity for intact porous Ti samples were found to be well predicted by the micromechanical model for an isotropic porous material with spherical pores (see Section 1 of Supplement for further details) [44]. The theoretical estimation of the intact Ti porous scaffolds, of which the average pore diameter is ~300 μm, shows good agreement with experimental measurement as shown in Fig. 5b. After densification, the pore structure was changed from sphere to flat pore, thus the measured stiffness of densified porous scaffolds deviated from the theoretical prediction with spherical pores. Instead, another micromechanical model for an isotropic pore material with flat pores has been introduced to predict the mechanical behavior of densified Ti scaffolds (see Section 1 of Supplement for further details) [44]. This flat pore model shows a better fit to the experimental data as seen in Fig. 5b. The ratio of the diameter to thickness for flat pores was assumed to be 0.03, which well corresponds to the microscopic observation in which the average diameter and thickness of the flat pores were roughly 300 μm and 10 μm, respectively as appears in Fig. 4c and Table 1.

Yield strength is also found to be controlled by the degree of densification as show in Fig. 5c. The initial yield strength of the intact porous scaffolds before densification is less than 150 MPa, whereas the densified scaffolds reach the maximum yield strength of 370 MPa at p = 7%. Furthermore, the densified scaffolds with increased yield strength were found to behave like an elastic body with full recovery below the yield strength even after multiple cycling loading.

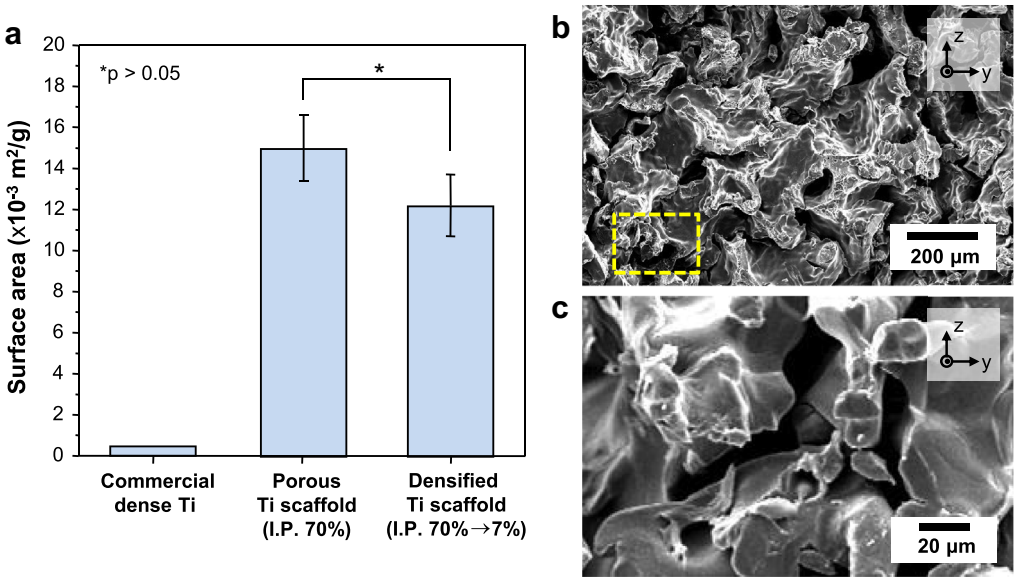

Fig. 4. (a) BET surface area of commercial dense, porous and densified Ti specimen and (b), (c) fractured cross-sectional SEM images of the densified Ti scaffold (I.P. = 70% and densified up to 7%) at (b) low and (c) high magnifications. The image of (c) was obtained from the region of (b), highlighted with the yellow dash box. The total surface area per weight of the porous Ti and its densified scaffolds are not significantly different. (For interpretation of the references to color in this figure legend, the reader is referred to the web version of this article.)

3.3. Controllable drug release behavior of densified Ti scaffolds

The loaded drug in this study was rhBMP-2, a bone growth factor in order to enhance the bone formation after metal implantation. Porous scaffolds with three different initial porosities were compared in terms of sustainability of drug release for 140 days while commercial dense titanium was set as the negative control. Fig. 6a shows the release behavior of rhBMP-2 from dense and porous titanium samples depending on porosity. Loaded rhBMP-2 on the commercial dense titanium was mostly released within 1 day while all porous Ti scaffolds before densification were found to release rapidly with almost 60% of loaded rhBMP-2 released on day 1 and then up to 90% by week 1. On the other hand, the densified porous scaffolds significantly exhibit more prolonged drug release behavior for 140 days with relatively consistent drug release on daily bases, alleviating the initial burst effect of drug release that is often observed among drug-loaded carriers.

Moreover, densification of porous scaffolds influenced the drug release behavior, as shown in Fig. 6b and c. Fig. 6b exhibits the relative release of rhBMP-2, normalized by the total loading amount for samples with three different porosities and corresponding densification. The relative drug release behavior of samples with three initial porosities before densification was found to be almost identical regardless of the porosity difference. This observation also appeared for the relative drug release behavior of three different initial porosities after densification up to the same final porosity, 7%. Therefore, the amount of loaded drug associated with the initial porosity was found to change the drug release rate as shown in Fig. 6a, but the relative release rate is independent of drug loading capacity. The degree of densification was a potential parameter to control drug release behavior as shown in Fig. 6c. The higher the degree of densification, the slower the drug release rate. The drug release behavior corresponding to the sample with densification of 7% was comparable to the intact sample, whereas about 25% decrease in porosity was found to produce more than 5× increase in the time for 80% drug release (~21 days) as compared to 7% decrease in porosity (~4 days).

The CLSM images of each Ti scaffold at day 0 clearly exhibit the distribution of GFP on the Ti surface (Fig. 7). The green (in the web version) signal of each image that is proportional to the amount of coated GFP is closely related to the porosity of the sample. The whole surface of dense Ti shows green signal, fully covered with GFP, whereas the porous Ti surface displays dark porous regions with green-colored struts where ~30% of the total surface is green. Densified porous Ti shows that more than 90% of the total area is green. As the release of GFP proceeded, the green signal was found to be significantly reduced. In particular, the surface of dense Ti became black after 14-day immersion, indicating that all GFP was fully released. In the case of porous Ti, after 14-day immersion, there was a small amount of GFP signal remnant, but the full release of GFP was observed after 56-day immersion. On the other hand, densified porous Ti consistently shows green signal until 112-day immersion, indicating the prolonged release of GFP. The different GFP release behavior depending on Ti scaffolds shows good agreement with the results of the rhBMP-2 release test.

3.4. Bioactivity improvement of rhBMP-coated Ti scaffolds

The densification process may have had an influence on the activities of the growth factors such as becoming inactive or denatured. Therefore, the denaturalization test was designed to confirm whether the growth factor is biologically active even after prolonged released from the scaffold. The differentiation levels of the cells that were cultured in the rhBMP-2 solution obtained on week 2, 4, 6 and 8 showed significantly higher levels of ALP activity when compared to that of the cells cultured in a medium without any rhBMP-2 supplements (negative control) as shown in Fig. 8a. The rhBMP-2 supplemented with fresh rhBMP-2 directly into the medium (positive control) promoted cell differentiation and showed higher levels of ALP activity when compared to the negative control. The cells that were cultured with the solutions containing rhBMP-2 released on week 2, 4, 6 and 8 showed a slightly decreased ALP activities, however all samples showed increased ALP activity when compared to that of the negative control.

Biological improvement associated with bioactive coating on metal scaffolds was demonstrated by *in vitro* cell test as well as *in vivo* animal test using a rabbit calvarial defect model. The *in vitro*

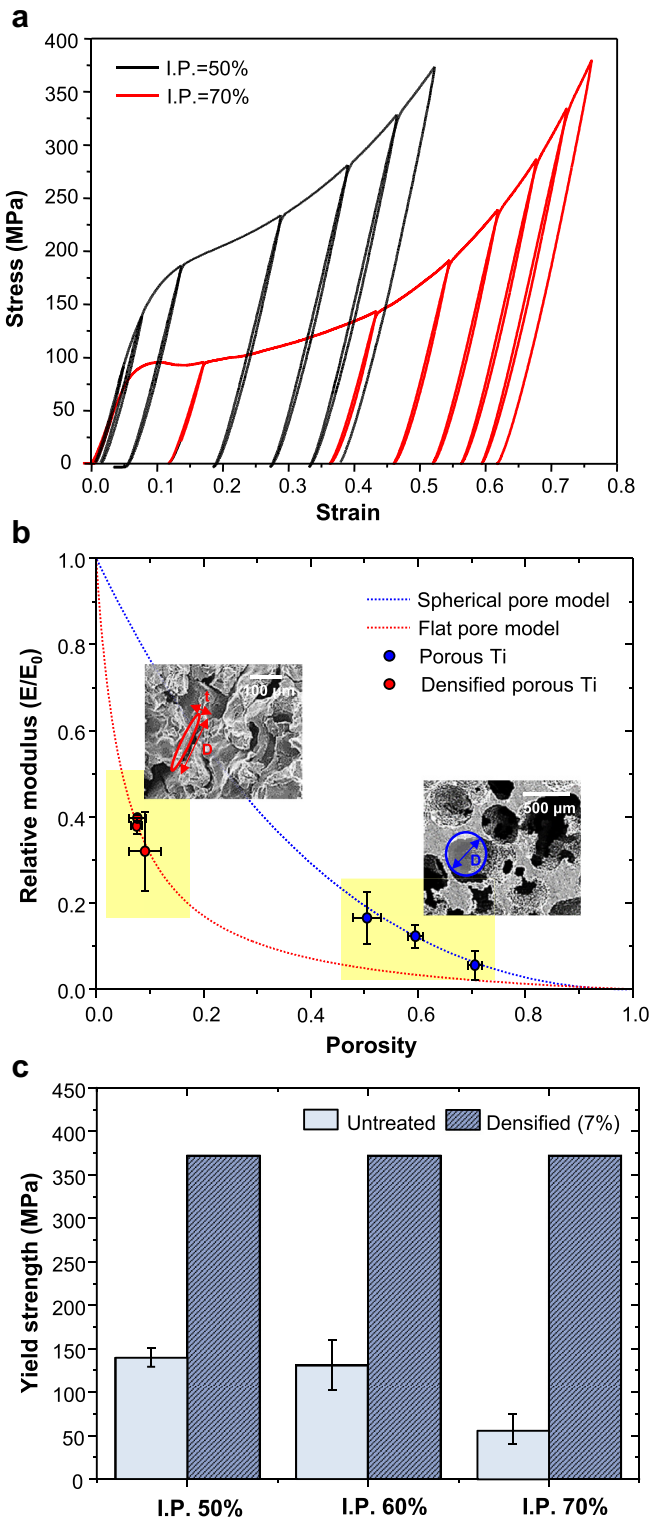

Fig. 5. (a) Representative stress–strain curves of porous Ti scaffolds (I.P. = 50% and 70%) under cyclic loading (b) Theoretical and experimental dependences of the ratios of the relative modulus of porous scaffold to the corresponding moduli of the dense body (Ti; $E_0 = 110$ GPa) on the porosity of the material and (c) yield strength of porous and densified scaffolds at three corresponding I.P. = 50, 60 and 70%. Inlet images of (b) indicate a typical microstructure of porous and densified samples with representative pore shapes (sphere for porous scaffold; ellipsoid for densified scaffold).

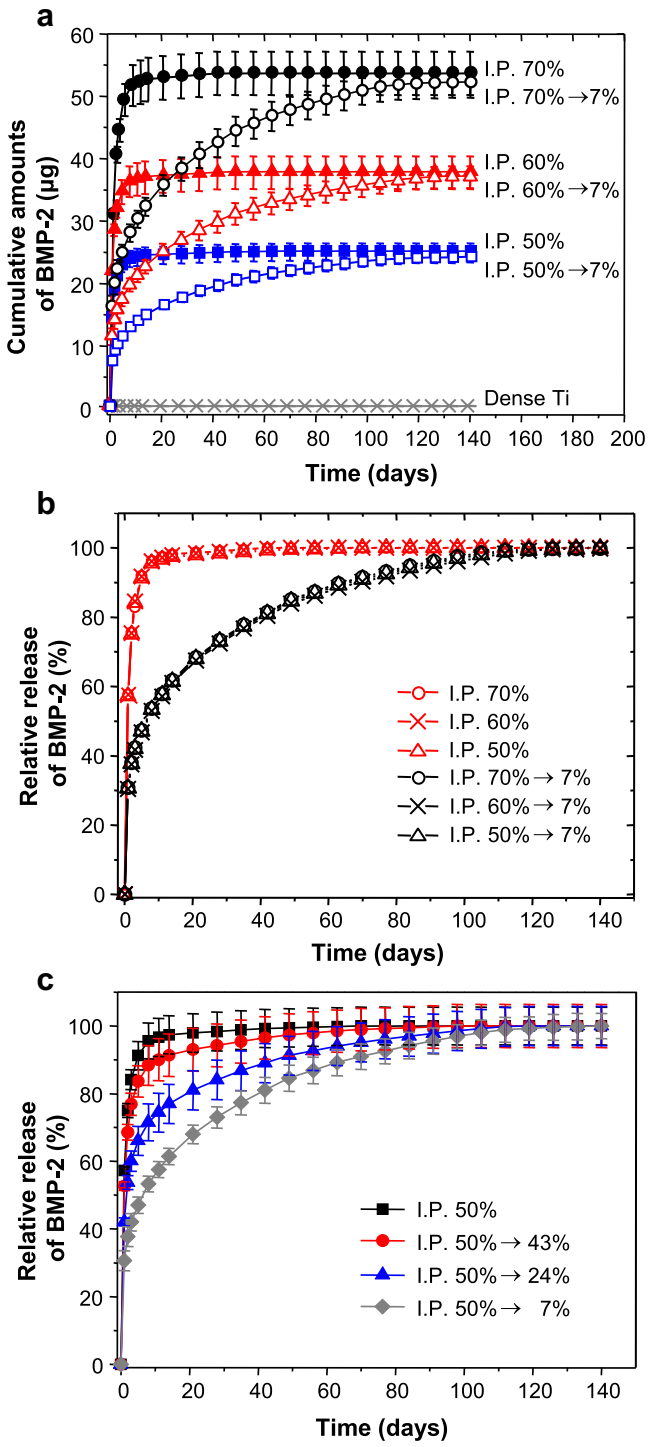

Fig. 6. (a) Cumulative amounts of growth factor (rhBMP-2) released from porous and densified Ti scaffolds as a function of time ($n = 5$) at I.P. = 50, 60 and 70%, as compared to those released from dense Ti, (b) relative release behavior of rhBMP-2 coated on porous and densified Ti scaffolds as a function of time at I.P. = 50, 60, and 70%, and (c) dependences of relative release behavior of rhBMP-2 released from Ti scaffolds on degree of densification at I.P. = 50%.

cellular responses of the densified porous Ti coated with rhBMP-2 were examined in terms of the cell proliferation and differentiation levels of pre-osteoblast cells as compared to those of commercial Ti with and without rhBMP. The cell viability and differentiation on different substrates was characterized with MTS assay and ALP activities on day 5 and day 10 of culturing as shown

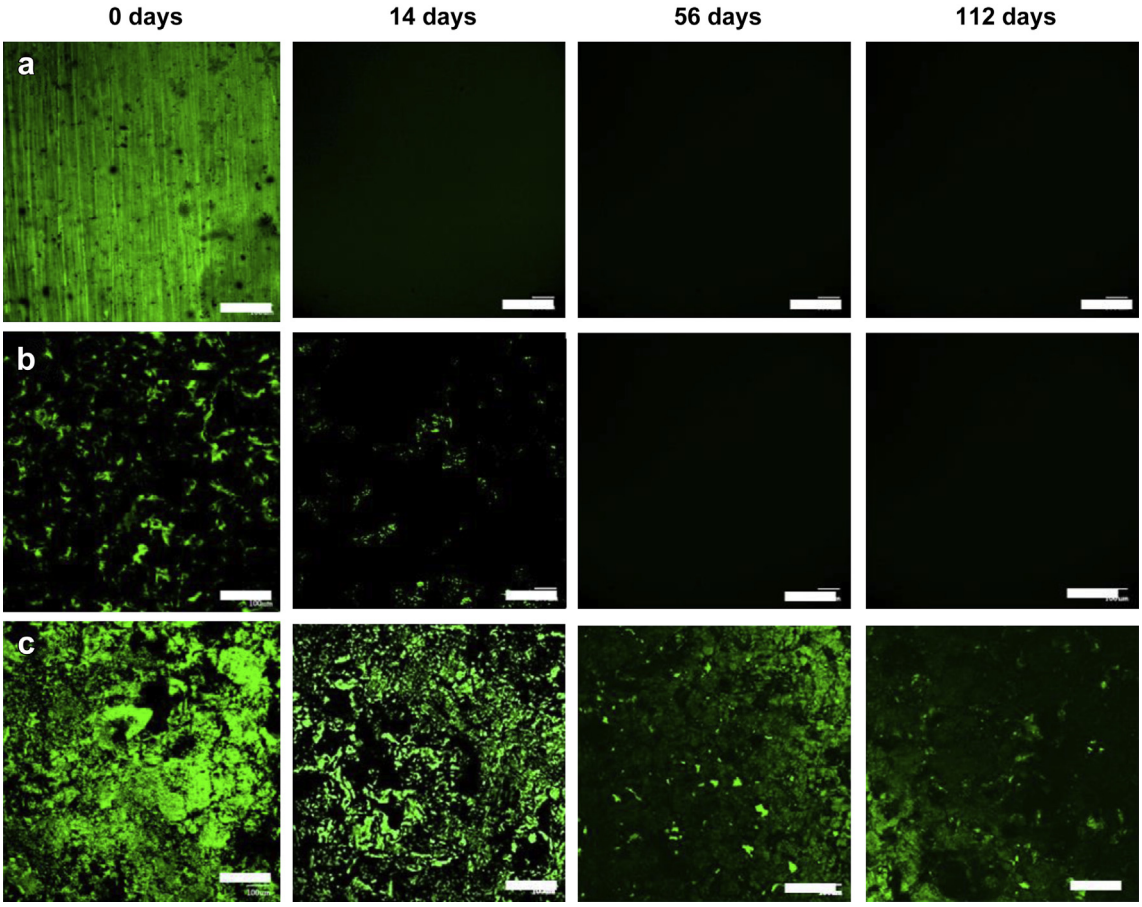

Fig. 7. Representative CLSM images of post-release surfaces of GFP loaded Ti scaffolds after immersed in PBS solution for 0, 14, 28 56, and 112 days for (a) commercial dense Ti, (b) porous Ti and (c) densified porous Ti (scale bar = 200 μm).

in Fig. 8b. After culturing for 5 days, it is worth noting that the cells that adhered to densified porous Ti coated with rhBMP-2 showed significantly higher cell viability than those of commercial Ti and rhBMP-2-adsorbed commercial Ti ($p < 0.05$). The result indicates that sufficient amounts of rhBMP-2 from densified porous Ti improved the cytocompatibility of Ti scaffolds. Moreover, the ALP activity of the cells on densified porous Ti coated with rhBMP-2 was significantly higher than that on the commercial Ti and rhBMP-2-adsorbed commercial Ti ($p < 0.05$).

For *in vivo* tests using a rabbit calvarial defect model, densified metallic scaffold with rhBMP-2 was compared to commercial dense titanium samples with or without the rhBMP-2 coating. Ring-type titanium samples (Fig. 9a) were implanted onto the calvarial defect area of a rabbit for 6 weeks, the duration of which significant osteoconductivity of loaded rhBMP-2 on the scaffolds were proved by previous studies [32,33]. During the test, no infections were observed in the defect regions and all animals were in good health conditions with no noticeable change in body weight and diet. After 6 weeks of implantation, all samples were retrieved and stained in order to evaluate the regenerated bone tissue around the implants. Representative histological cross-section images of the implanted titanium samples are shown in Fig. 9b in which two black squares correspond to cross-sections of each titanium ring and porous red (in the web version) regions are the calvarial bone tissue. Bone was newly formed around all titanium implants, indicating the signs of osteoconduction, whereas the coverage and volume of newly formed bone was found to vary depending on the samples. The role of rhBMP-2 is clearly shown when comparing dense titanium samples with and without rhBMP-2. The commercial dense titanium ring coated with rhBMP-2 showed more bone surrounding the sample, including the inner surface as well as the top surface of the ring, compared to the titanium without coating. Furthermore, the densified porous titanium with rhBMP-2 exhibits the largest volume and coverage of bone with the surface of its ring covered with the newly formed bone, and the new bone is found to diffuse from the edge of the inner ring surface to the defect region as shown in Fig. 10a. A quantitative analysis of the new bone generation in the interior of implanted Ti rings was performed via image analysis using μ-CT images (Fig. 10a). The densified porous titanium with rhBMP-2 was found to possess a significantly large bone volume (9.6 ± 3.0 mm^3) when compared to other dense titanium samples (0.8 ± 0.1 mm^3 for no coating, and 2.6 ± 0.7 mm^3 for rhBMP-2 coating), as shown in Fig. 10b. Therefore, the significantly improved osteoconductivity of the densified samples with rhBMP-2 implies the effect of sustainable rhBMP-2 release over the implantation period.

4. Discussion

Even though biometals have been widely used for biomedical applications, there is still room for improvement because of mechanical mismatch and low bioactivity. In particular, recent studies that focus on the surface modification of grafting materials for inducing rapid bone ingrowth have utilized stimulatory molecules, which includes peptides, proteins, and growth factors on the surface that enables quicker and more stable cell colonization [45,46].

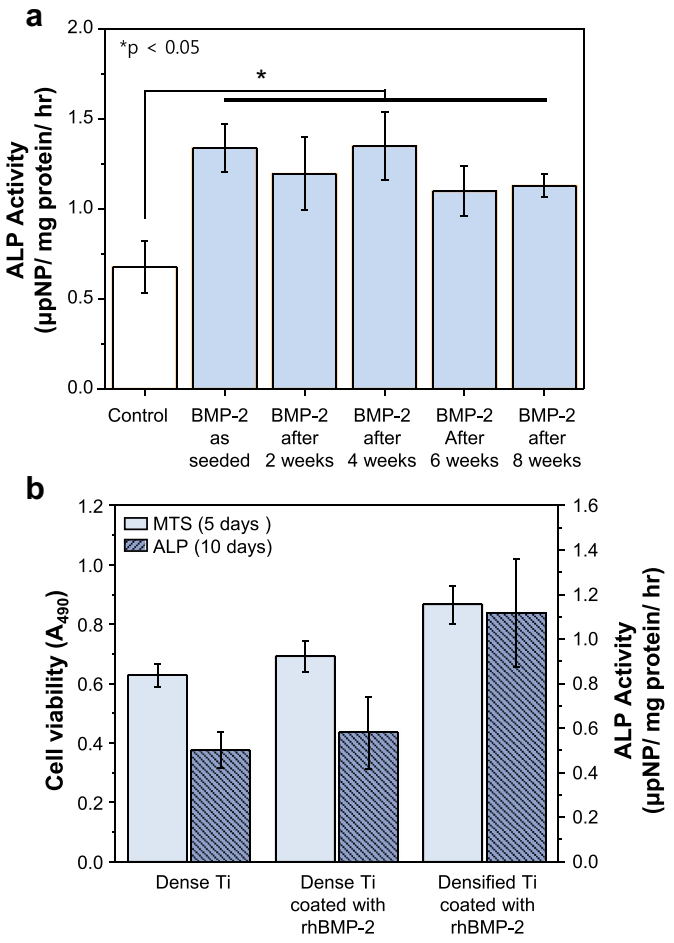

Fig. 8. (a) *In vitro* ALP activity test of MC3T3 cells cultured in 6-well plates with culturing medium supplemented with the released solutions from rhBMP-2-coated densified Ti scaffolds after different release times (2, 4, 6 and 8 weeks) was compared to the activity of cells cultured without rhBMP-2 (negative), and (b) cell proliferation and ALP activity of MC3T3-E1 cells of commercial Ti, rhBMP-2 coated commercial Ti and rhBMP-2-coated densified Ti after culturing for 5 and 10 days. All values of Fig. 8b are significantly different ($p < 0.05$) except for the pair of dense Ti and rhBMP-2 coated Ti for ALP activity data.

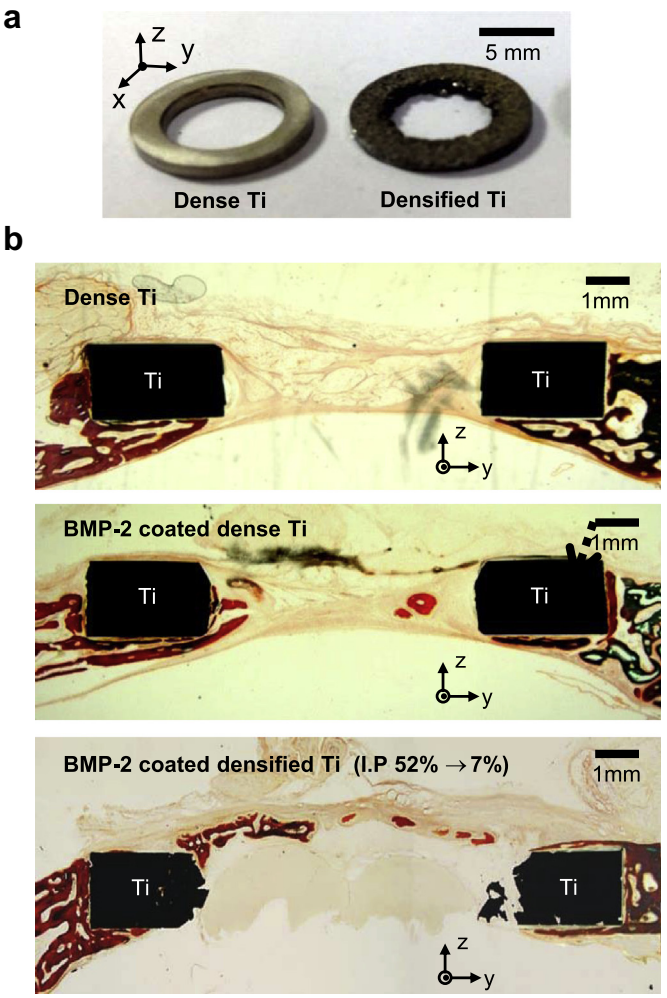

Fig. 9. (a) Ring-type Ti implants made of the dense body and densified scaffold (I.P. = 50% and densified up to 7%) for *in vivo* test, and (b) optical images of a representative rabbit calvaria after 6 weeks of healing with dense Ti (top), dense Ti with rhBMP-2 coating (middle) and densified porous Ti with rhBMP-2 coating (bottom). Arrows indicate the newly grown bone around the implants.

Considerable effort has been devoted to ensure the stable localization of bioactive molecules using either a physical adsorption or chemical crosslinking methods [47,48]. Physical adsorption has limitations since using soluble growth factor may not be sufficient for long-term implantation due to protein desorption and/or exchange with physiologic fluid contact. Moreover, several studies suggested that micro pores on the surface or porous structure can be used to sustain growth factor release [49–51]. To our knowledge, no studies have been performed to study the effects of deformed porous structures following adsorption of growth factor onto the pore walls.

Designing a scaffold that can deliver BMP-2 to promote quicker bone regeneration needs to consider the following requirements: (a) supplying of BMP-2 in a biologically relevant manner, (b) providing osteogenic stimulations through direct biochemical/biomechanical signaling, (c) retaining a porous, osteoconductive surface that supports cell attachment and cell infiltration, and (d) maintaining sufficient mechanical strength for the surgical application. Various materials such as poly-DL-lactic acid scaffolds, nanofibrous chitosan membrane, polylactide/glycolide polymers, and nanohydroxyapatite/collagen/poly-L-lactic acid scaffolds have been used as BMP carriers [52–55]. In previous studies, BMPs have been incorporated into implants in various ways: infused in titanium sponges, covalently bonded through chromosulfuric acid treatment, impregnated in hydroxyapatite plasma-sprayed around implants, and soaked in polylactic acid membranes [17,56–58]. In this work, porous titanium has been selected as a BMP-2 carrier where rhBMP-2 was loaded into the pores and the pore structure was further modified through densification for sustained release of rhBMP-2.

Common methods of fabricating porous titanium include space holder method, replication of polymeric sponge, freeze casting and sintering of metal particles [22–24,59]. The porosity and pore size can be controlled by various parameters adapted in aforementioned methods. Recently, rapid prototyping (RP) has attracted much attention as a method for manufacturing porous material with tailorable pore structure [8,60–62]. Mechanical stability of porous metals largely depends on chemical contamination or structural irregularities during the fabrication of porous scaffolds [20,23]. In particular, porous metals with high pore interconnectivity are often more susceptible to those chemical and structural impurities. From our previous study [42], the dynamic freezing casting method was found to produce porous Ti scaffolds that possess high pore interconnectivity, yet good ductility under compression with negligible organic contamination. The ductility of porous Ti samples is a key enabler that allows the large

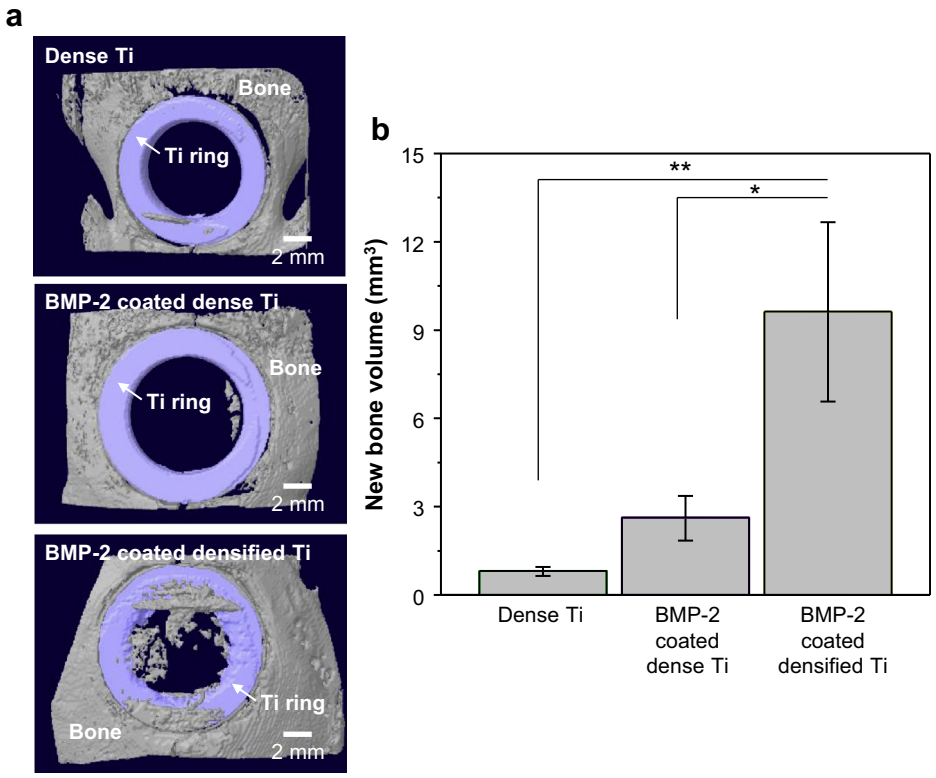

Fig. 10. (a) 3D reconstructions of Ti implants embedded in rabbit calvaria after 6 week implantation using μ-CT data for commercial dense Ti (top), commercial dense Ti coated with rhBMP-2 (middle) and densified porous Ti coated with rhBMP-2 (bottom), and (b) quantification of new bone on the top and internal parts of the Ti rings after 6 week implantation, determined by μ-CT analysis ($^{*}p < 0.01$, $^{**}p < 0.001$).

deformation of the struts, enabling the densification of the porous samples without abrupt collapse or catastrophic failure. In this study, more than 90% samples fabricated by the dynamic freezing casting were successfully densified by >90% of initial porosity without fracture. Further densification (F.P. <7%) was not observed under feasible pressure conditions because the bent struts started contacting each other, giving increased resistance against pressure. Moreover, the deformed microstructure of densified porous scaffolds exhibits minimal influence on the overall pore connectivity, indicating no apparent decrease of surface area as compared to that of the intact porous sample.

The major advantage of metallic porous body is reduced stiffness which is comparable to that of biological hard tissues, minimizing stress shield effects [63–65]. In particular, mechanical performance of porous scaffolds show great dependency on porosity, pore structure and distribution [42,66,67], and, in turn, the densification of the porous scaffolds is seen to change porosity and pore structure (Figs. 3 and 4). As shown in Fig. 5b, stiffness predicted by the spherical pore model exhibits a moderate increase as the porosity decreases, reaching a half level of the stiffness of the fully dense body at the porosity of ~25%. On the other hand, the flat pore model shows a sharp increase of the stiffness at the porosity <10% while the relative stiffness of the porous samples is predicted to be less than 0.3 at the porosity >10%. Thus, even though the densification process is able to produce highly densified porous scaffolds up to $p = 7\%$, the increased stiffness has the upper limit that is less than a half of the stiffness of the fully dense body because of the changed pore structures. Elastic modulus of densified Ti scaffolds was found to lie between ~5 GPa ($p = 70\%$) and ~40 GPa ($p = 7\%$) depending on the degree of densification, which is comparable to that of bone (3–20 GPa) [2,68,69]. This finding suggests that stress shielding, generally observed for dense Ti implants with a relatively high elastic modulus (~100 GPa [70]), can be effectively mitigated, which would, in turn, provide excellent long-term stability *in vivo*. It should be noted that the mechanical strength can be tailored for specific applications simply by adjusting the level of densification without serious stress shielding. Therefore, through the densification, the porous scaffolds vary from load bearing elastic supporters with high stiffness and high yield strength, to energy dissipation mediator with low stiffness and low yield strength, exhibiting mechanical tunability in response to the design requirements of orthopedic applications.

Bone morphogenetic protein-2 (BMP-2) has been widely used to accelerate the healing process of bone defects and is also used in medical and dental implants [32,34,35]. Therefore, many studies have incorporated BMP-2 in implants to stimulate and augment bone formation more quickly. However, some negative side effects including heterotopic bone formation, retrograde ejaculation and osteoclast activation were found when supraphysiologic doses of BMP-2 were delivered over relatively short periods [31,36–38,40]. The development of a carrier system that is capable of a sustained and controlled release of biologically active BMP-2 over an extended period is a goal that many researchers are trying to meet to devise an ideal growth factor releasing system [39–41]. Various materials which include synthetic polymers, natural polymers and calcium phosphate have been proposed and investigated for use as BMP carriers on metal surfaces [12,32,71–73]. However, in many cases, BMP-2 adsorbed superficially on the metal surfaces releases with an initial burst and diffuses away from the implantation site too quickly.

Densified titanium scaffolds were found to control rhBMP-2 release through two main parameters, initial porosity and degree of densification, reducing the initial burst effect with the enhanced release period. First, the initial porosity is closely related to drug

loading capacity. With scaffolds of the same weight, the increase in initial porosity improves drug loading capacity from ~0.03 μg rhBMP-2/g titanium (0% porosity) to ~18.55 μg rhBMP-2/g titanium (70% porosity) by a factor of ~720, which was considerably augmented, relative to the difference of surface area (30×) as shown in Fig. 6a. The external surface of a specimen is more vulnerable to rhBMP-2 loss following multiple cleaning steps after a drug loading process than the internal surface. Therefore, the drug loading capacity of a porous scaffold likely depends on the internal surface area which is increased by initial porosity. It is found that 10% increase of the initial porosity leads to about 50% increase of drug loading capacity. Second, a more densified pore structure has longer release period because of the associated microstructural changes. The dissolved rhBMP-2 diffuses to the outside medium through a concentration gradient. From Fig. 6b and c, for 80% drug release, relative tortuosity factors were calculated as compared with the case of the intact sample with the initial porosity of 50%, using Higuchi's diffusion model with the assumption that the diffusion coefficient for all cases is identical (see Section 2 of Supplement for further details) [74,75]. As shown in Fig. 11, relative tortuosity factors were significantly increased up to ~20 after densification to porosity of ~7%, associated with the prolonged drug release period. Porous scaffolds with the porosity of more than 50% exhibit almost identical relative tortuosity factors to the scaffold with 50% porosity, indicating that in this regime, tortuosity has minimal effect on drug release rates (Fig. 6c) and instead, the amount of drug loading is the dominant parameter for drug release behavior (Fig. 6a). Therefore, densification was found to increase tortuosity, implying that the degree of densification for porous scaffolds is the major parameter to control the drug release behavior.

It is expected that titanium implants containing and continuously releasing rhBMP-2 will enhance bone formation at the implant surface and promote faster bone regeneration at the injured site. Many research demonstrated that rhBMP-2 plays a critical role in up-regulating transient PI3 kinase and Akt kinase which in turn shows enhanced cell viability, proliferation and migration [76–78]. We hypothesized that the long-term release of growth factor will promote faster bone generation which will be reflected in *in vitro* and *in vivo* tests. The densified Ti with the lowest porosity of (F.P. = 7%) was employed to be examined for *in vitro* and *in vivo* tests, since it showed the longest drug-release period (c.f. Fig. 6c), which is one of the most important

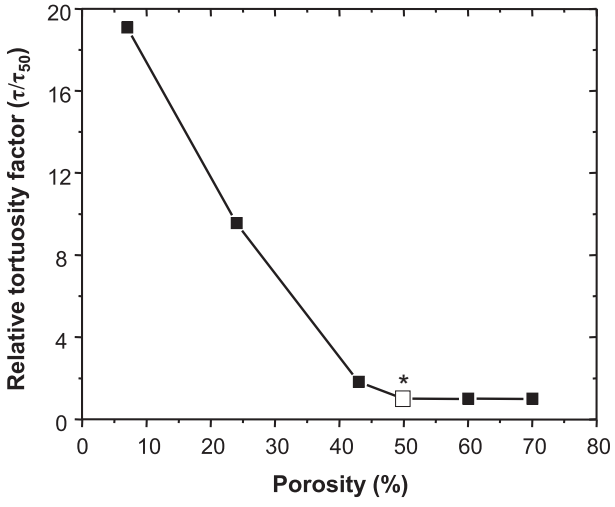

Fig. 11. Relative tortuosity factors of porous and densified scaffolds to the porous scaffold with I.P. = 50%.

requirements for successful osseo-integration *in vivo*, as well as reasonable mechanical properties (high strength and low stiffness) for load-bearing applications. The denaturalization tests clearly showed that rhBMP-2 released from the densified porous samples is bioactive even after 8 weeks of release, successfully inducing differentiation of cells (Fig. 9a). The *in vitro* cellular responses of Ti scaffolds with or without rhBMP-2 also indicate that proliferation and differentiation of cells on densified porous Ti with rhBMP-2 were significantly improved as compared to those of commercial Ti. In particular, commercial Ti coated with rhBMP-2 was found to exhibit the similar level of cell viability and ALP activity to commercial Ti without rhBMP-2. From the release test, the release behavior of rhBMP-2 from the commercial Ti was found to display the initial bursting effect and relatively short release period (<3 days) as compared to porous or densified porous Ti scaffolds. The *in vivo* tests further proved the improved bioactivity of densified porous Ti with rhBMP-2. Qualitative and quantitative results of *in vivo* tests showed that the contact area and volume of newly formed bone on the surface of densified porous Ti with BMP-2 loading were significantly larger than those of dense Ti samples without and even with BMP-2 loading. This remarkable improvement in osseo-integration, the direct structural and functional connection between the surface of an implant and living bone [79,80], was mainly attributed to the sustained release of BMP-2 from the densified Ti. In addition, a rough surface with residual pores after densification process can contribute to the improved osseo-integration ability of the densified Ti through by providing mechanical interlocking [81]. It should be noted that the porosity and pore size of densified Ti scaffolds can be increased by decreasing the level of densification, which would, accordingly, effectively induce bone ingrowth if necessary. The *in vitro* and *in vivo* test results presented in this study suggest that BMP-2-releasing densified porous Ti may have potential for future dental and orthopedic materials. Although we only tested rhBMP-2 as a sample growth factor, the presented delivery system can be utilized with other growth factors and drugs for localized delivery of substances.

The densification of porous Ti scaffolds could allow for significantly improved mechanical properties and sustained release of BMP-2 over a prolonged period of time. However, this densification process would decrease the pore size of porous Ti scaffolds, accordingly, limiting bone ingrowth into pores. In order for further optimization, the process we developed can be extended to tailor the design of a metallic body in response to various conditions in terms of mechanical performance, drug release rate and pore size. In particular, by varying the height, the potential design of a metallic body leads to various graded porous structures that possess differentiation of porosity, stiffness and strength as well as drug release behavior depending on the level of densification and can be easily fabricated by compressing a mechanically machined porous scaffold that exhibits spatial height variation. The schematic design proposed in Fig. 12a shows the structure with a porous inner layer surrounded by a dense outer layer. The dense layer of the structure possesses a longer drug release duration, supporting the whole structure with stiffer and stronger mechanical properties, whereas the porous inner layer allows the cell migration from the top or bottom surfaces and promotes tissue ingrowth with larger pore size. The effective mechanical properties follow the rule of mixture, being proportional to the volume ratios of dense and porous layers. It should be noted that densified Ti scaffolds with sufficiently large pores for bone ingrowth can provide much higher mechanical strength and toughness than bioceramic scaffolds (e.g. calcium phosphate), which would allow them to be used for load-bearing applications.

A Ti scaffold corresponding to the schematic design was fabricated by means of the dynamic freeze casting as shown in Fig. 12a.

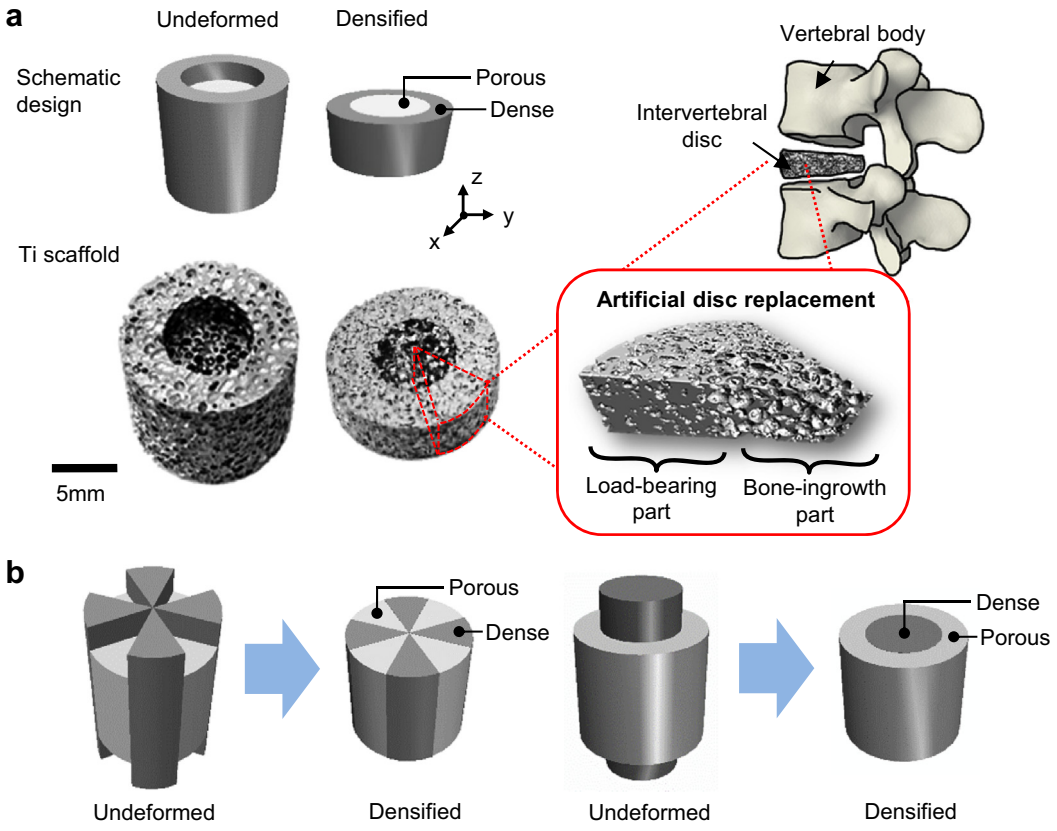

Fig. 12. (a) Schematic of a scaffold design with gradient porosity (top) and the corresponding Ti scaffold fabricated through densification (bottom) in which the scaffold possesses a porous internal core surrounded by the densified outer layer as artificial disc replacement, and (b) schematics of additional potential porous scaffold designs varying porosity, degree of densification and structures.

Through machining, heights of the cylindrical Ti porous scaffold with I.P. = 70% were varied, where the height of the outer layer was three times longer than that of the inner layer, leading to two different strains ($\varepsilon = 0.05, 0.68$) during densification under uniaxial compression. The densified porous sample successfully possesses the double-layered structure: the outer layer with the porosity of ~8% and flat pores and the inner layer with the porosity of ~68% with spherical pores as shown from the μ-CT image in Fig. 12a. Depending on the initial porosity, length of layers and degree of densification, multi-layered porous structures can be customized to vary the mechanical properties and drug release behavior. This graded porous metallic body has great potential as orthopedic applications, e.g., artificial disc replacement as indicated in Fig. 12a. The dense outer layer provides mechanical support while the porous inner layer allows the transport of cells and mediums.

Moreover, additional schematic designs for graded porous structures have been proposed in Fig. 12b. The radial pattern of the first design provides the porous and dense structures alternatively, which allows the mixed performance of two structures in space, whereas the second design may alter the roles of outer and inner layers of Fig. 12a, imposing different functionality. The densification process for the application of porous scaffolds as a drug carrier as well as a mechanical supporter can be applied to other metal systems besides Ti. Ductility of a metallic porous body is a key factor to enable the densification process. Currently, the dynamic freeze casting is a potential fabrication method of a metallic porous body that achieves good ductility of the scaffold with minimal contamination and structural instability. However, because densification is proposed as a post-treatment process after a porous scaffold is fully formed, it can be introduced to any fabrication methods of a metallic scaffold in which optimal processing conditions improve the ductility of the scaffold.

5. Conclusions

Densified porous titanium was successfully fabricated, where the degree of densification was controlled by the applied strain under uniaxial compression. During densification, structural integrity of porous titanium was well maintained without any mechanical deterioration under various cyclic loading conditions, exhibiting good pore connectivity and large surface area. Densified porous titanium possesses two important features that have not been achieved by either dense titanium or porous titanium: 1) mechanical tunability of porous scaffolds through densification that allows scaffolds to be applied ranging from highly porous fillers to dense load-bearing implants and 2) improved bioactivity of titanium through bioactive coating that is capable of sustainable release through utilizing high surface area and pore connectivity with controllable tortuosity of densified porous scaffolds. Densification of porous scaffolds can also be applied to the fabrication of functionally graded porous scaffolds by spatially varied strain during densification. This simple, but effective post-fabrication process of porous scaffolds has great potential as a method to resolve unmet needs of biometallic materials as various biomedical applications.

Acknowledgments

This research was supported by the Technology Innovation Program (Contract grant No. 0037915, WPM Biomedical

Materials—Implant Materials) funded by the Ministry of Knowledge Economy (MKE, Korea). Also, L.F. Wang acknowledges the support of the National Science Foundation (CMMI-1437449).

Appendix A. Supplementary data

Supplementary data related to this article can be found online at http://dx.doi.org/10.1016/j.biomaterials.2014.10.027.

References

[1] Long M, Rack H. Titanium alloys in total joint replacement-a materials science perspective. Biomaterials 1998;19:1621–39.
[2] Niinomi M. Recent metallic materials for biomedical applications. Metal Mater Trans A 2002;33:477–86.
[3] Frosch KH, Stürmer KM. Metallic biomaterials in skeletal repair. Eur J Trauma 2006;32:149–59.
[4] Huiskes R, Weinans H, Van Rietbergen B. The relationship between stress shielding and bone resorption around total hip stems and the effects of flexible materials. Clin Orthop Relat Res 1992;274:124–34.
[5] Kanayama M, Cunningham BW, Haggerty CJ, Abumi K, Kaneda K, McAfee PC. In vitro biomechanical investigation of the stability and stress-shielding effect of lumbar interbody fusion devices. J Neurosurg Spine 2000;93:259–65.
[6] Jung H-D, Kim H-E, Koh Y-H. Production and evaluation of porous titanium scaffolds with 3-dimensional periodic macrochannels coated with microporous TiO2 layer. Mater Chem and Phys 2012;135:897–902.
[7] Jones AC, Arns CH, Sheppard AP, Hutmacher DW, Milthorpe BK, Knackstedt MA. Assessment of bone ingrowth into porous biomaterials using MICRO-CT. Biomaterials 2007;28:2491–504.
[8] Li JP, Habibovic P, van den Doel M, Wilson CE, de Wijn JR, van Blitterswijk CA, et al. Bone ingrowth in porous titanium implants produced by 3D fiber deposition. Biomaterials 2007;28:2810–20.
[9] Ahn M-K, Jo I-H, Koh Y-H, Kim H-E. Production of highly porous titanium (Ti) scaffolds by vacuum-assisted foaming of titanium hydride (TiH_2) suspension. Mater Lett 2014;120:228–31.
[10] Bobyn J, Stackpool G, Hacking S, Tanzer M, Krygier J. Characteristics of bone ingrowth and interface mechanics of a new porous tantalum biomaterial. J Bone Joint Surg Br 1999;81:907–14.
[11] Li H, Yuan B, Gao Y, Chung CY, Zhu M. Remarkable biocompatibility enhancement of porous NiTi alloys by a new surface modification approach: in-situ nitriding and in vitro and in vivo evaluation. J Biomed Mater Res Part A 2011;99:544–53.
[12] Baas J, Elmengaard B, Jensen TB, Jakobsen T, Andersen NT, Soballe K. The effect of pretreating morselized allograft bone with rhBMP-2 and/or pamidronate on the fixation of porous Ti and HA-coated implants. Biomaterials 2008;29:2915–22.
[13] Peng L, Bian W-g, Liang F-h, Xu H-z. Implanting hydroxyapatite-coated porous titanium with bone morphogenetic protein-2 and hyaluronic acid into distal femoral metaphysis of rabbits. Chin J Traumatol (English Edition) 2008;11:179–85.
[14] Reiner T, Kababya S, Gotman I. Protein incorporation within Ti scaffold for bone ingrowth using Sol-gel SiO2 as a slow release carrier. J Mater Sci Mater Med 2008;19:583–9.
[15] Jansen J, Vehof J, Ruhe P, Kroeze-Deutman H, Kuboki Y, Takita H, et al. Growth factor-loaded scaffolds for bone engineering. J Control Release 2005;101:127–36.
[16] Clark PA, Moioli EK, Sumner DR, Mao JJ. Porous implants as drug delivery vehicles to augment host tissue integration. FASEB J 2008;22:1684–93.
[17] Lan J, Wang Z, Shi B, Xia H, Cheng X. The influence of recombinant human BMP-2 on bone–implant osseointegration: biomechanical testing and histomorphometric analysis. Int J Oral Maxillofac Surg 2007;36:345–9.
[18] Freilich M, M Patel C, Wei M, Shafer D, Schleier P, Hortschansky P, et al. Growth of new bone guided by implants in a murine calvarial model. Bone 2008;43:781–8.
[19] Yoo JJ, Park Y-J, Rhee S-H, Chun HJ, Kim HJ. Synthetic peptide-conjugated titanium Alloy for enhanced bone formation in vivo. Connect Tissue Res 2012;53:359–65.
[20] Liu P, Tan Q, Wu L, He G. Compressive and pseudo-elastic hysteresis behavior of entangled titanium wire materials. Mater Sci Eng A 2010;527:3301–9.
[21] Cay H, Xu H, Li Q. Mechanical behavior of porous magnesium/alumina composites with high strength and low density. Mater Sci Eng A 2013;574:137–42.
[22] Lee JH, Kim HE, Shin KH, Koh YH. Improving the strength and biocompatibility of porous titanium scaffolds by creating elongated pores coated with a bioactive, nanoporous TiO2 layer. Mater Lett 2010;64:2526–9.
[23] Li JC, Dunand DC. Mechanical properties of directionally freeze-cast titanium foams. Acta Mater 2011;59:146–58.
[24] Kim SW, Jung H-D, Kang M-H, Kim H-E, Koh Y-H, Estrin Y. Fabrication of porous titanium scaffold with controlled porous structure and net-shape using magnesium as spacer. Mater Sci Eng C. 2013;33:2808–15.
[25] Kato K, Yamamoto A, Ochiai S, Wada M, Daigo Y, Kita K, et al. Cytocompatibility and mechanical properties of novel porous 316L stainless steel. Mater Sci Eng C 2013;33:2736–43.
[26] Gao Y, Zhu S, Luo E, Li J, Feng G, Hu J. Basic fibroblast growth factor suspended in Matrigel improves titanium implant fixation in ovariectomized rats. J Control Release 2009;139:15–21.
[27] Jiang QH, Liu L, Peel S, Yang GL, Zhao SF, He FM. Bone response to the multilayer BMP-2 gene coated porous titanium implant surface. Clin Oral Implants Res 2013;24:853–61.
[28] Han CM, Jang TS, Kim HE, Koh YH. Creation of nanoporous TiO2 surface onto polyetheretherketone for effective immobilization and delivery of bone morphogenetic protein. J Biomed Mater Res Part A 2014;102:793–800.
[29] Von Walter M, Herren C, Gensior T, Steffens G, Hermanns-Sachweh B, Jahnen-Dechent W, et al. Biomimetic modification of the TiO_2/glass composite Ecopore with heparinized collagen and the osteoinductive factor BMP-2. Acta Biomater 2008;4:997–1004.
[30] Tayalia P, Mooney DJ. Controlled growth factor delivery for tissue engineering. Adv Mater 2009;21:3269–85.
[31] Zara JN, Siu RK, Zhang X, Shen J, Ngo R, Lee M, et al. High doses of bone morphogenetic protein 2 induce structurally abnormal bone and inflammation in vivo. Tissue Eng Part A 2011;17:1389–99.
[32] Jun S-H, Lee E-J, Jang T-S, Kim H-E, Jang J-H, Koh Y-H. Bone morphogenic protein-2 (BMP-2) loaded hybrid coating on porous hydroxyapatite scaffolds for bone tissue engineering. J Mater Sci Mater Med 2013:1–10.
[33] Jung HD, Yook SW, Han CM, Jang TS, Kim HE, Koh YH, et al. Highly aligned porous Ti scaffold coated with bone morphogenetic protein-loaded silica/chitosan hybrid for enhanced bone regeneration. J Biomed Mater Res Part B Appl Biomat 2014;102:913–21.
[34] Yamaguchi A, Katagiri T, Ikeda T, Wozney JM, Rosen V, Wang EA, et al. Recombinant human bone morphogenetic protein-2 stimulates osteoblastic maturation and inhibits myogenic differentiation in vitro. J Cell Biol 1991;113:681–7.
[35] Katagiri T, Yamaguchi A, Komaki M, Abe E, Takahashi N, Ikeda T, et al. Bone morphogenetic protein-2 converts the differentiation pathway of C2C12 myoblasts into the osteoblast lineage. J Cell Biol 1994;127:1755–66.
[36] Smucker JD, Rhee JM, Singh K, Yoon ST, Heller JG. Increased swelling complications associated with off-label usage of rhBMP-2 in the anterior cervical spine. Spine 2006;31:2813–9.
[37] Wong DA, Kumar A, Jatana S, Ghiselli G, Wong K. Neurologic impairment from ectopic bone in the lumbar canal: a potential complication of off-label PLIF/TLIF use of bone morphogenetic protein-2 (BMP-2). Spine J 2008;8:1011–8.
[38] Carragee EJ, Mitsunaga KA, Hurwitz EL, Scuderi GJ. Retrograde ejaculation after anterior lumbar interbody fusion using rhBMP-2: a cohort controlled study. Spine J 2011;11:511–6.
[39] Coombes A, Meikle M. Resorbable synthetic polymers s replacements for bone graft. Clin Mater 1994;17:35–67.
[40] Burg KJL, Porter S, Kellam JF. Biomaterial developments for bone tissue engineering. Biomaterials 2000;21:2347–59.
[41] Takahashi Y, Yamamoto M, Tabata Y. Enhanced osteoinduction by controlled release of bone morphogenetic protein-2 from biodegradable sponge composed of gelatin and β-tricalcium phosphate. Biomaterials 2005;26:4856–65.
[42] Jung H-D, Yook S-W, Jang T-S, Li Y, Kim H-E, Koh Y-H. Dynamic freeze casting for the production of porous titanium (Ti) scaffolds. Mater Sci Eng C. 2013;33:59–63.
[43] Jun S-H, Lee E-J, Kim H-E, Jang J-H, Koh Y-H. Silica-chitosan hybrid coating on Ti for controlled release of growth factors. J Mater Sci Mater Med 2011;22:2757–64.
[44] Koval'chenko M. Mechanical properties of isotropic porous materials. I. Elastic and rheological properties. Powder Metall Metal Ceram 1993;32:268–73.
[45] Hanisch O, Sorensen RG, Kinoshita A, Spiekermann H, Wozney JM, Wikesjö UME. Effect of recombinant human BMP-2 in dehiscence defects with non-submerged immediate implants: an experimental study in Cynomolgus monkeys. J Periodontol 2003;74:648–57.
[46] Morra M, Cassinelli C, Meda L, Fini M, Giavaresi G, Giardino R. Surface analysis and effects on interfacial bone microhardness of collagen-coated titanium implants: a rabbit model. Int J Oral Maxillofac Implants 2005;20:23.
[47] Wikesjö UME, Lim WH, Thomson RC, Cook AD, Wozney JM, Hardwick WR. Periodontal repair in dogs: evaluation of a bioabsorbable space-providing macro-porous membrane with recombinant human bone morphogenetic protein-2. J Periodontol 2003;74:635–47.
[48] Tessmar J, Kellner K, Schulz MB, Blunk T, Göpferich A. Toward the development of biomimetic polymers by protein immobilization: PEGylation of insulin as a model reaction. Tissue Eng 2004;10:441–53.
[49] Yang G, He F, Hu J, Wang X, Zhao S. Effects of biomimetically and electrochemically deposited nano-hydroxyapatite coatings on osseointegration of porous titanium implants. Oral Surg Oral Med Oral Pathol, Oral Radiol, Endodontol 2009;107:782–9.
[50] Lee J, Decker JF, Polimeni G, Cortella CA, Rohrer MD, Wozney JM, et al. Evaluation of implants coated with rhBMP-2 using two different coating strategies: a critical-size supraalveolar peri-implant defect study in dogs. J Clin Periodontol 2010;37:582–90.
[51] So K, Takemoto M, Fujibayashi S, Neo M, Kokubo T, Nakamura T. Reinforcement of tendon attachment to bioactive porous titanium by BMP-2-induced ectopic bone formation. J Biomed Mater Res Part A 2010;93:1410–6.

[52] Yang XB, Whitaker MJ, Sebald W, Clarke N, Howdle SM, Shakesheff KM, et al. Human osteoprogenitor bone formation using encapsulated bone morphogenetic protein 2 in porous polymer scaffolds. Tissue Eng 2004;10:1037–45.
[53] Jones AA, Buser D, Schenk R, Wozney J, Cochran DL. The effect of rhBMP-2 around endosseous implants with and without membranes in the canine model. J Periodontol 2006;77:1184–93.
[54] Park YJ, Kim KH, Lee JY, Ku Y, Lee SJ, Min BM, et al. Immobilization of bone morphogenetic protein-2 on a nanofibrous chitosan membrane for enhanced guided bone regeneration. Biotechnol Appl Biochem 2006;43:17–24.
[55] Zhang C, Hu YY, Cui FZ, Zhang SM, Ruan DK. A study on a tissue-engineered bone using rhBMP-2 induced periosteal cells with a porous nano-hydroxyapatite/collagen/poly (L-lactic acid) scaffold. Biomed Mater 2006;1:56.
[56] Kawai T, Mieki A, Ohno Y, Umemura M, Kataoka H, Kurita S, et al. Osteoinductive activity of composites of bone morphogenetic protein and pure titanium. Clin Orthop Relat Res 1993;290:296.
[57] Sachse A, Wagner A, Keller M, Wagner O, Wetzel WD, Layher F, et al. Osteointegration of hydroxyapatite-titanium implants coated with non-glycosylated recombinant human bone morphogenetic protein-2 (BMP-2) in aged sheep. Bone 2005;37:699–710.
[58] Becker J, Kirsch A, Schwarz F, Chatzinikolaidou M, Rothamel D, Lekovic V, et al. Bone apposition to titanium implants biocoated with recombinant human bone morphogenetic protein-2 (rhBMP-2). A pilot study in dogs. Clin Oral Investig 2006;10:217–24.
[59] Oh I-H, Nomura N, Hanada S. Microstructures and mechanical properties of porous titanium compacts prepared by powder sintering. Mater Trans 2002;43:443–6.
[60] Wiria FE, Shyan JYM, Lim PN, Wen FGC, Yeo JF, Cao T. Printing of Titanium implant prototype. Mater Des 2010;31:S101–5.
[61] Hollister SJ. Scaffold design and manufacturing: from concept to clinic. Adv Mater 2009;21:3330–42.
[62] Hutmacher DW. Scaffolds in tissue engineering bone and cartilage. Biomaterials 2000;21:2529–43.
[63] Engh C, Bobyn J, Glassman A. Porous-coated hip replacement. The factors governing bone ingrowth, stress shielding, and clinical results. J Bone Joint Surg Br 1987;69:45–55.
[64] Ryan G, Pandit A, Apatsidis DP. Fabrication methods of porous metals for use in orthopaedic applications. Biomaterials 2006;27:2651–70.
[65] Krishna BV, Bose S, Bandyopadhyay A. Low stiffness porous Ti structures for load-bearing implants. Acta Biomater 2007;3:997–1006.
[66] Simone A, Gibson L. Effects of solid distribution on the stiffness and strength of metallic foams. Acta Mater 1998;46:2139–50.
[67] Gibson LJ. Biomechanics of cellular solids. J Biomech 2005;38:377–99.
[68] Katti KS. Biomaterials in total joint replacement. Colloids Surfaces B Biointerfaces 2004;39:133–42.
[69] Staiger MP, Pietak AM, Huadmai J, Dias G. Magnesium and its alloys as orthopedic biomaterials: a review. Biomaterials 2006;27:1728–34.
[70] Shen H, Oppenheimer SM, Dunand DC, Brinson LC. Numerical modeling of pore size and distribution in foamed titanium. Mech Mater 2006;38:933–44.
[71] Bae SE, Choi J, Joung YK, Park K, Han DK. Controlled release of bone morphogenetic protein (BMP)-2 from nanocomplex incorporated on hydroxyapatite-formed titanium surface. J Control Release 2012;160:676–84.
[72] Vo TN, Kasper FK, Mikos AG. Strategies for controlled delivery of growth factors and cells for bone regeneration. Adv Drug Deliv Rev 2012;64:1292–309.
[73] Lee HJ, Koo AN, Lee SW, Lee MH, Lee SC. Catechol-functionalized adhesive polymer nanoparticles for controlled local release of bone morphogenetic protein-2 from titanium surface. J Control Release 2013;170:198–208.
[74] Higuchi T. Mechanism of sustained-action medication. Theoretical analysis of rate of release of solid drugs dispersed in solid matrices. J Pharm Sci 1963;52:1145–9.
[75] Higuchi T. Rate of release of medicaments from ointment bases containing drugs in suspension. J Pharm Sci 1961;50:874–5.
[76] Armstrong L, Hughes O, Yung S, Hyslop L, Stewart R, Wappler I, et al. The role of PI3K/AKT, MAPK/ERK and NFκβ signalling in the maintenance of human embryonic stem cell pluripotency and viability highlighted by transcriptional profiling and functional analysis. Hum Mol Genet 2006;15:1894–913.
[77] Vandermoere F, El Yazidi-Belkoura I, Demont Y, Slomianny C, Antol J, Lemoine J, et al. Proteomics exploration reveals that actin is a signaling target of the kinase Akt. Mol Cell Proteomics 2007;6:114–24.
[78] Vandermoere F, El Yazidi-Belkoura I, Slomianny C, Demont Y, Bidaux G, Adriaenssens E, et al. The valosin-containing protein (VCP) is a target of Akt signaling required for cell survival. J Biol Chem 2006;281:14307–13.
[79] Branemark PI. Osseointegration and its experimental background. J Prosthet Dent 1983;50:399–410.
[80] Gotz HE, Muller M, Emmel A, Holzwarth U, Erben RG, Stangl R. Effect of surface finish on the osseointegration of laser-treated titanium alloy implants. Biomaterials 2004;25:4057–64.
[81] Grizon F, Aguado E, Hure G, Basle MF, Chappard D. Enhanced bone integration of implants with increased surface roughness: a long term study in the sheep. J Dent 2002;30:195–203.